CONF-9604171--1

SHELL-MODEL MONTE CARLO METHODS

S. E. Koonin
California Institute of Technology
Pasadena, CA 91125

and

D. J. Dean
Oak Ridge National Laboratory*
Oak Ridge, TN 37831

to be published in

Proceedings of Contemporary Shell Model Workshop

Philadelphia, PA
April 29-30, 1996

*Managed by Lockheed Martin Energy Research Corp. under contract DE-AC05-96OR22464 with the U.S.D.O.E.

DISCLAIMER

Shell Model Monte Carlo Methods

Steven E. Koonin[1] and David J. Dean[2]

[1] W.K. Kellogg Radiation Laboratory, California Institute of Technology, Pasadena, CA 91125 USA
[2] Physics Division, Oak Ridge National Laboratory Oak Ridge, TN 37831 USA

Abstract. We review quantum Monte Carlo methods for dealing with large shell model problems. These methods reduce the imaginary-time many-body evolution operator to a coherent superposition of one-body evolutions in fluctuating one-body fields; the resultant path integral is evaluated stochastically. We first discuss the motivation, formalism, and implementation of such Shell Model Monte Carlo (SMMC) methods. There then follows a sampler of results and insights obtained from a number of applications. These include the ground state and thermal properties of *pf*-shell nuclei, the thermal behavior of γ-soft nuclei, and the calculation of double beta-decay matrix elements. Finally, prospects for further progress in such calculations are discussed.

1 Introduction

The description of nuclear structure began more than 60 years ago with the discovery of the neutron. Major milestones were the discovery of single-particle shells (1), collective motion (2), and their reconciliation (3). However, a number of recent developments impose new and more stringent tests of our ability to describe nuclear structure. Heavy-ion induced reactions allow the study of nuclear behavior at extremes of temperature, angular momentum, or isospin (4). Increasingly precise experiments with electron (5), pion (6), kaon (7, 8), and nucleon (9, 10) beams probe new modes of excitation. As our understanding of supernovae (11) and nucleosynthesis (12) is refined there is a corresponding need to know more precisely the relevant nuclear properties. Furthermore, new pictures of nuclear structure such as the Interacting Boson Model (13) make implicit or explicit assumptions about the solutions of the underlying fermion problem that demand verification.

The range and diversity of nuclear behavior (perhaps the greatest of any quantal many-body system) have naturally engendered a host of models. Short of a complete solution to the many-nucleon problem (14), the interacting shell model is widely regarded as the most broadly capable description of low-energy nuclear structure, and the one most directly traceable to the fundamental many-body problem. Many studies have demonstrated that exact diagonalizations of shell-model Hamiltonians can accurately and consistently describe a wide range of nuclear properties, *if* the many-body basis is sufficiently large. Pioneering papers include work in the $0p$ (15), $0s$-$1d$ (16) and $0f_{7/2}$ (17) shells; more recent examples are given in Refs. (18, 19, 20). Unfortunately, the combinatorial scaling

of the many-body space with the size of the single particle basis or the number of valence nucleons restricts such exact diagonalizations to either light nuclei or to heavier nuclei with only a few valence particles (21).

The Shell Model Monte Carlo (SMMC) methods have been developed in the past few years (22, 23, 24, 25, 26) to circumvent some of these difficulties while retaining the rigor, flexibility, and predictive power of traditional shell model calculations. These methods are based on a Monte Carlo evaluation of the path integral obtained by a Hubbard-Stratonovich (HS) transformation (27) of the imaginary-time evolution operator. The many-body problem is thus reduced to a set of one-body problems in fluctuating auxiliary fields (28). The method enforces the Pauli principle exactly, and the storage and computation time scale gently with the single-particle basis or the number of particles. Auxiliary field methods have been applied to condensed matter systems such as the Hubbard Model (29, 30), yielding important information about electron correlations and magnetic properties.

Our presentation is organized as follows. In section 2 we review the rationale and definition of the interacting shell model and some of the important characteristics of the two-body interaction. In section 3, we give an overview of SMMC methods, showing how the HS transformation can be used to express physically interesting observables as ratios of high-dimensional integrals. In section 4, we discuss the various ways in which a realistic shell model Hamiltonian can be cast in a form suitable for the HS transform. In section 5 we discuss the notorious sign problems and a practical method for their solution as well as the validation of the overall method. section 6 is a sampler of various types of SMMC calculations (virtually all intractable by other methods), and in section 7 we offer a perspective on future work.

2 Review of the shell model

In this section, we present a brief definition and overview of the nuclear shell model. Our goals are to establish conventions and notation and to give the non-expert some appreciation for the special features of the nuclear problem relative to other quantal many-body systems. More detailed discussions can be found in several texts (3, 31, 32, 33, 34).

The notion of independent particles moving in a common one-body potential is central to our description of atoms, metals, and hadrons. It is also realized in nuclei, and the shell structure associated with the magic numbers was first put on a firm basis in 1949, when the magic numbers were explained by an harmonic oscillator spectrum with a strong, inverted (with respect to the atomic case) spin-orbit potential (1).

But nuclei differ from the other quantal systems cited above in that the residual interaction between the valence fermions is strong and so severely perturbs the naive single-particle picture. This interaction mixes together many different configurations to produce the true eigenstates and, because of its coherence,

there emerge phenomena such as pairing, modification of sum rules, deformation, and collective rotations and vibrations. An accurate treatment of the residual interaction is therefore essential to properly describe nuclei.

The nuclear shell model is defined by a set of spin-orbit coupled single-particle states with quantum numbers ljm denoting the orbital angular momentum (l) and the total angular momenta (j) and its z-component, m. Although non-spherical one-body potentials are a common efficiency used in describing deformed nuclei, for the rotationally invariant Hamiltonians used in SMMC so far, these states have energies ε_{lj} that are independent of m. The single-particle states and energies may be different for neutrons and protons, in which case it is convenient to include also the isospin component $t_3 = \pm 1/2$ in the state description. We will use the label α for the set of quantum numbers ljm or $ljmt_3$, as appropriate.

The particular single-particle states included in a given calculation depend upon the physics being addressed, but at least one major shell is believed to be necessary to adequately describe low-lying states of a given nucleus. We will use N_s to denote the number of such states. Thus, for example, N_s is (12, 20, 32, 44) for either neutrons or protons in the ($1s0d$, $1p0f$, $2s1dg_{7/2}h_{11/2}$, $2p1fh_{9/2}i_{13/2}$) shells.

The totality of Pauli-allowed configurations of the valence nucleons in the single particle states defines the model space in which the many-body Hamiltonian acts. Computing the dimension of this space (number of such many-body states) is a straightforward combinatorial exercise. As noted in the Introduction, the dimension increases strongly with either N_s or the number of valence nucleons, and can vastly exceed 10^8 for realistic applications of current interest. The size of the Hamiltonian matrix to be considered can be reduced somewhat by exploiting rotational and isospin invariance properties. Even so, constructing such a matrix and finding its lowest eigenvalues and eigenstates is difficult in some cases of interest and impossible in most, and thermal properties are completely inaccessible without *ad hoc* assumptions.

The shell model Hamiltonian can be written in the form $\hat{H} = \hat{H}_1 + \hat{H}_2$ where

$$\hat{H}_1 = \sum_\alpha \varepsilon_\alpha a^\dagger_\alpha a_\alpha \ , \tag{2.1a}$$

$$\hat{H}_2 = \frac{1}{2} \sum_{\alpha\beta\gamma\delta} V_{\alpha\beta\gamma\delta} a^\dagger_\alpha a^\dagger_\beta a_\delta a_\gamma \ . \tag{2.1b}$$

Here, $a^\dagger$ and a are fermion creation and annihilation operators, and the V are the uncoupled matrix elements of the two-body interaction. These latter must respect rotational and time-reversal invariance, parity conservation, and in many cases isospin invariance. To make explicit the rotational and isospin invariance, and shell structure, we can rewrite the two-body Hamiltonian as

$$\hat{H}_2 = \frac{1}{4} \sum_{abcd} \sum_{JT} [(1+\delta_{ab})(1+\delta_{cd})]^{1/2} V^N_{JT}(ab,cd) \sum_{MTz} \hat{A}^\dagger_{JT;MTz}(ab) \hat{A}_{JT;MTz}(cd) \ , \tag{2.2}$$

where the pair operator is

$$\hat{A}^{\dagger}_{JT;MTz}(ab) = \sum_{m_a,m_b} (j_a m_a j_b m_b | JM)(\frac{1}{2} t_a \frac{1}{2} t_b | TT_z) a^{\dagger}_{j_b m_b t_b} a^{\dagger}_{j_a m_a t_a} \ . \qquad (2.3)$$

Here $(\frac{1}{2}, t_a)$, etc. are the isospin indices with $t_a = -\frac{1}{2}$ for proton states and $t_a = \frac{1}{2}$ for neutron states, and (TT_z) are the coupled isospin quantum numbers, and the sum is taken over all proton and neutron single-particle orbits (denoted by a, b, c, d).

The $V_{JT}(ab, cd)$ are the angular-momentum and isospin coupled two-body matrix elements (TBME) of a scalar potential $V(\mathbf{r}_1, \mathbf{r}_2)$ defined as

$$V_{JT}(ab, cd) = \langle [\psi_{j_a}(\mathbf{r}_1) \times \psi_{j_b}(\mathbf{r}_2)]^{JMTT_z} | V(\mathbf{r}_1, \mathbf{r}_2) | [\psi_{j_c}(\mathbf{r}_1) \times \psi_{j_d}(\mathbf{r}_2)]^{JMTT_z} \rangle \ , \qquad (2.4)$$

(independent of M and T_z). In this isospin formalism, since $\hat{A}_{JT;MTz}(ab) = (-1)^{j_a+j_b-J+T} \hat{A}_{JT;MTz}(ba)$, the definitions of the symmetric and antisymmetric parts of $V^N_{JT}(ab, cd)$, $V^S_{JT}(ab, cd)$, and $V^A_{JT}(ab, cd)$ become

$$V^{S/A}_{JT}(ab, cd) \equiv \frac{1}{2} \left[V^N_{JT}(ab, cd) \pm (-1)^{J+j_a+j_b+T-1} V^N_{JT}(ba, cd) \right] \ . \qquad (2.5)$$

There are a number of methods for deriving the residual interaction V (which acts in the model space) from the underlying "bare" internucleon interaction (35, 36, 37). Although a complete specification of V requires many two-body matrix elements (38, 39) (e.g., 63 in the complete *sd*-shell and 195 in the complete *pf*-shell), successful interactions that reproduce a large body of experimental data show a few simple features (e.g., isoscalar pairing, attractive quadrupole, repulsive dipole, ...), with the rest of the TBMEs being small and random (39, 40). A venerable approximation is to truncate the interaction to just the isoscalar pairing and the quadrupole interaction (41).

In conventional shell model applications the dimension of the model space makes a complete diagonalization of the Hamiltonian impractical. As one is usually interested only in the nuclear spectrum at low energies, the diagonalization is often performed using the Lanczos algorithm, which is an efficient way to find the few lowest (or highest) eigenvalues and eigenvectors of a large matrix (43, 44).

Beyond the *sd*-shell, applications of the conventional shell model become more problematic as the large dimensions of the model space make diagonalization impossible. To date, systematic studies of the $A = 48$ isobars, involving model spaces with about 10^6 Slater determinants, have been the limit for the conventional shell model approaches (45). Nevertheless the successful description of these nuclei underlines again that the shell model concept is also the method of choice in heavier nuclei – if such applications were only possible. As noted by Caurier *et al.* (45), it took two generations of hardware and software development to extend shell model calculations from $A = 44$ to $A = 48$. Thus, conventional shell model calculations for nuclei heavier than $A = 50$ appear out of reach in the near future, even assuming an optimistic increase of computer capabilities.

3 Overview of Monte Carlo methods

In this section, we give an overview of SMMC methods. In particular, we describe what the methods are (and are not) capable of calculating. We then discuss the essence of the HS transformation, which is at the heart of the calculations.

The SMMC methods rely on an ability to deal with the imaginary-time many-body evolution operator, $\exp(-\beta\hat{H})$, where β is a real c-number. While this does not result in a complete solution to the many-body problem in the sense of giving all eigenvalues and eigenstates of $\hat{H}$, it can result in much useful information. For example, the expectation value of some observable $\hat{\Omega}$ in the grand canonical ensemble can be obtained by adding to $\hat{H}$ a term $-\mu_n\hat{N} - \mu_p\hat{Z}$, ($\mu_n$ and μ_p are the neutron and proton chemical potentials) and then calculating

$$\langle\hat{\Omega}\rangle = \frac{\mathrm{Tr}\, e^{-\beta\hat{H}}\hat{\Omega}}{\mathrm{Tr}\, e^{-\beta\hat{H}}} \,. \tag{3.1}$$

Here, $\beta \equiv T^{-1}$ is interpreted as the inverse of the temperature T, and the many-body trace is defined as

$$\mathrm{Tr}\,\hat{X} \equiv \sum_i \langle i|\hat{X}|i\rangle \,, \tag{3.2}$$

where the sum is over *all* many-body states of the system. Similarly, if $\hat{P}_A = \delta(A - \hat{N})$ is the projector onto states with A nucleons (actually the product of separate neutron and proton projectors), the canonical ensemble is defined by

$$\mathrm{Tr}_A\,\hat{X} \equiv \sum_i \langle i|\hat{P}_A\hat{X}|i\rangle \,, \tag{3.3}$$

and the associated expectation value is

$$\langle\hat{\Omega}\rangle_A = \frac{\mathrm{Tr}_A\, e^{-\beta\hat{H}}\hat{\Omega}}{\mathrm{Tr}_A\, e^{-\beta\hat{H}}} \,. \tag{3.4}$$

In the limit of low temperature ($T \to 0$ or $\beta \to \infty$), both the grand-canonical and canonical traces reduce to ground state expectation values. Alternatively, if $|\Phi\rangle$ is a many-body trial state not orthogonal to the exact ground state, $|\Psi\rangle$, then $e^{-\beta\hat{H}}$ can be used as a filter to refine $|\Phi\rangle$ to $|\Psi\rangle$ as β becomes large. An observable can be calculated in this "zero temperature" method as

$$\frac{\langle\Phi|e^{-\frac{\beta}{2}\hat{H}}\hat{\Omega}e^{-\frac{\beta}{2}\hat{H}}|\Phi\rangle}{\langle\Phi|e^{-\beta\hat{H}}|\Phi\rangle} \underset{\beta\to\infty}{} \frac{\langle\Psi|\hat{\Omega}|\Psi\rangle}{\langle\Psi|\Psi\rangle} \,. \tag{3.5}$$

If $\hat{\Omega}$ is the Hamiltonian, then (3.5) at $\beta = 0$ is the variational estimate of the energy, and improves as β increases. Of course, the efficiency of the refinement for any observable depends upon the degree to which $|\Phi\rangle$ approximates $|\Psi\rangle$.

Beyond such static properties, $e^{-\beta\hat{H}}$ allows us to obtain some information about the dynamical response of the system. For operators $\Omega^\dagger$ and Ω, the response function $R_\Omega(\tau)$ in the canonical ensemble is defined as

$$R_\Omega(\tau) \equiv \frac{\mathrm{Tr}_A\, e^{-(\beta-\tau)\hat{H}}\hat{\Omega}^\dagger e^{-\tau\hat{H}}\hat{\Omega}}{\mathrm{Tr}_A\, e^{-\beta\hat{H}}} \equiv \langle\hat{\Omega}^\dagger(\tau)\hat{\Omega}(0)\rangle_A, \tag{3.6}$$

where $\hat{\Omega}^\dagger(\tau) \equiv e^{\tau\hat{H}}\hat{\Omega}^\dagger e^{-\tau\hat{H}}$ is the imaginary-time Heisenberg operator. As we shall see in section 8 below, interesting choices for $\hat{\Omega}$ are the a_j for particular orbitals, the Gamow-Teller, $M1$, or quadrupole moment, etc. Inserting complete sets of A-body eigenstates of $\hat{H}$ ($\{|i\rangle, |f\rangle\}$ with energies $E_{i,f}$) shows that

$$R_\Omega(\tau) = \frac{1}{Z}\sum_{if} e^{-\beta E_i}|\langle f|\hat{\Omega}|i\rangle|^2 e^{-\tau(E_f-E_i)}, \tag{3.7}$$

where $Z = \sum_i e^{-\beta E_i}$ is the partition function. Thus, $R_\Omega(\tau)$ is the Laplace transform of the strength function $S_\Omega(E)$:

$$R_\Omega(\tau) = \int_{-\infty}^{\infty} e^{-\tau E} S_\Omega(E)dE\ , \tag{3.8a}$$

$$S_\Omega(E) = \frac{1}{Z}\sum_{fi} e^{-\beta E_i}|\langle f|\hat{\Omega}|i\rangle|^2\delta(E-E_f+E_i)\ . \tag{3.8b}$$

Hence, if we can calculate $R_\Omega(\tau)$, $S_\Omega(E)$ can be determined by a full inversion of the Laplace transform using Maximum Entropy techniques (22). Short of this inversion (which is often numerically difficult), the behavior of $R_\Omega(\tau)$ for small τ gives information about the energy-weighted moments of S_Ω. In particular,

$$R_\Omega(0) = \int_{-\infty}^{\infty} S_\Omega(E)dE = \frac{1}{Z}\sum_i e^{-\beta E_i}|\langle f|\hat{\Omega}|i\rangle|^2 = \langle\hat{\Omega}^\dagger\hat{\Omega}\rangle_A \tag{3.9}$$

is the total strength,

$$-R'_\Omega(0) = \int_{-\infty}^{\infty} S_\Omega(E)EdE = \frac{1}{Z}\sum_{if} e^{-\beta E_i}|\langle f|\hat{\Omega}|i\rangle|^2(E_f-E_i) \tag{3.10}$$

is the first moment, and so on. (In these expressions, the prime denotes differentiation with respect to τ.)

It is important to note that we cannot usually obtain detailed spectroscopic information from SMMC calculations. Rather, we can calculate expectation values of operators in the thermodynamic ensembles or the ground state. Occasionally, these can indirectly furnish properties of excited states. For example, if there is a collective 2^+ state absorbing most of the $E2$ strength, then the centroid of the quadrupole response function will be a good estimate of its energy. But, in general, we are without the numerous specific excitation energies and wavefunctions that characterize a direct diagonalization. This is both a blessing and a

curse. The former is that for the very large model spaces of interest, there is no way in which we can deal explicitly with all of the wavefunctions and excitation energies. Indeed, we often don't need to, as experiments only measure average nuclear properties at a given excitation energy. The curse is that comparison with detailed properties of specific levels is difficult. In this sense, the SMMC method is complementary to direct diagonalization for modest model spaces, but is the only method for treating very large problems.

It remains, of course, to describe the Hubbard-Stratanovich "trick" by which $e^{-\beta\hat{H}}$ is managed. In broad terms, the difficult many-body evolution is replaced by a superposition of an infinity of tractable one-body evolutions, each in a different external field, σ. Integration over the external fields thus reduces the many-body problem to quadrature.

For a realistic Hamiltonian, there will be many non-commuting density operators $\hat{\mathcal{O}}_\alpha$ present, but we will always be able to reduce the two-body term to diagonal form, as discussed in section 4. Thus for a general two-body interaction in a general time-reversal invariant form, we write

$$\hat{H} = \sum_\alpha \left(\epsilon^*_\alpha \hat{\bar{\mathcal{O}}}_\alpha + \epsilon_\alpha \hat{\mathcal{O}}_\alpha \right) + \frac{1}{2} \sum_\alpha V_\alpha \left\{ \hat{\mathcal{O}}_\alpha, \hat{\bar{\mathcal{O}}}_\alpha \right\} , \tag{3.11}$$

where $\hat{\bar{\mathcal{O}}}_\alpha$ is the time reverse of $\hat{\mathcal{O}}_\alpha$. Since, in general $[\hat{\mathcal{O}}_\alpha, \hat{\mathcal{O}}_\beta] \neq 0$, we must split the interval β into N_t "time slices" of length $\Delta\beta \equiv \beta/N_t$,

$$e^{-\beta\hat{H}} = [e^{-\Delta\beta\hat{H}}]^{N_t}, \tag{3.12}$$

and for each time slice $n = 1, \ldots, N_t$ perform a linearization similar to (3.16) using auxiliary fields $\sigma_{\alpha n}$:

$$\begin{aligned} e^{-\Delta\beta\hat{H}} &\approx \int_{-\infty}^{\infty} \prod_n \left(\frac{d\sigma_{\alpha n} d\sigma^*_{\alpha n} \Delta\beta |V_\alpha|}{2\pi} \right) e^{-\Delta\beta \sum_\alpha |V_\alpha| |\sigma_{\alpha n}|^2} e^{-\Delta\beta \hat{h}_n} , \\ \hat{h}_n &= \sum_\alpha \left(\varepsilon^*_\alpha + s_\alpha V_\alpha \sigma_{\alpha n} \right) \hat{\bar{\mathcal{O}}}_\alpha + \left(\varepsilon_\alpha + s_\alpha V_\alpha \sigma^*_{\alpha n} \right) \hat{\mathcal{O}}_\alpha . \end{aligned} \tag{3.13}$$

Note that because the various $\hat{\mathcal{O}}_\alpha$ need not commute, (3.13) is accurate only through order $\Delta\beta$ and that the representation of $e^{-\Delta\beta\hat{h}}$ must be accurate through order $\Delta\beta^2$ to achieve that accuracy.

Upon composing (3.13) many times according to (3.12), we can write expressions for observables as the ratio of two field integrals. For example, (3.4) becomes

$$\langle \hat{\Omega} \rangle_A = \frac{\int \mathcal{D}\sigma W_\sigma \Omega_\sigma}{\int \mathcal{D}\sigma W_\sigma}, \tag{3.14a}$$

where

$$\begin{aligned} W_\sigma &= G_\sigma \mathrm{Tr}_A \hat{U} ; \qquad G_\sigma = e^{-\Delta\beta \sum_{\alpha n} |V_\alpha| |\sigma_{\alpha n}|^2} , \\ \Omega_\sigma &= \frac{\mathrm{Tr}_A \hat{U} \hat{\Omega}}{\mathrm{Tr}_A \hat{U}} ; \qquad \mathcal{D}\sigma \equiv \prod_{n=1}^{N_t} \prod_\alpha d\sigma_{\alpha n} d\sigma^*_{\alpha n} \left(\frac{\Delta\beta |V_\alpha|}{2\pi} \right) , \end{aligned} \tag{3.14b}$$

and

$$\hat{U} = \hat{U}_{N_t} \ldots \hat{U}_2 \hat{U}_1 \; ; \qquad \hat{U}_n = e^{-\Delta\beta \hat{h}_n} \; ,$$
$$\hat{h}_n = \sum_\alpha (\varepsilon^*_\alpha + s_\alpha V_\alpha \sigma_{\alpha n}) \hat{\mathcal{O}}_\alpha + (\varepsilon_\alpha + s_\alpha V_\alpha \sigma^*_{\alpha n}) \mathcal{O}_\alpha \; . \qquad (3.14c)$$

This is, of course, a discrete version of a path integral over σ. Because there is a field variable for each operator at each time slice, the dimension of the integrals $\mathcal{D}\sigma$ can be very large, often exceeding 10^5. Note that because of the errors in (3.13), the errors in Eqs. (3.14) are of order $\Delta\beta$, so that high accuracy requires large N_t and perhaps extrapolation to $N_t = \infty$ ($\Delta\beta = 0$).

An expression of the form (3.14) has a number of attractive features. First, the problem has been reduced to quadrature—we need only calculate the ratio of two integrals. Second, all of the quantum mechanics (which appears in Ω_σ) is of the one-body variety, which is simply handled by the algebra of $N_s \times N_s$ matrices. The price to pay is that we must treat the one-body problem for all possible σ fields.

In the following two sections we discuss the appropriate form for the Hamiltonian, and formulate the MC quadrature, respectively.

4 Decomposition of the Hamiltonian

We note that the two-body Hamiltonian for fermion systems is completely specified by the set of anti-symmetrized two-body matrix elements $V^A_{JT}(ab, cd)$ of Eq. (2.5) that are the input to many standard shell model codes such as OXBASH (42). The two-body Hamiltonian can now be written solely in terms of density operators that conserve the proton and neutron numbers. Namely,

$$\hat{H}_2 = \hat{H}'_1 + \hat{H}'_2 \; , \qquad (4.1)$$

where

$$\hat{H}'_1 = \sum_{ad} \sum_{t=p,n} \epsilon'_{ad} \rho_{0\,0t}(a,d) \; , \qquad (4.2)$$

with

$$\epsilon'_{ad} = -\frac{1}{4} \sum_b \sum_J (-1)^{J+j_a+j_b} (2J+1) \frac{1}{\sqrt{2j_a+1}} V^N_{JT=1}(ab,bd) \sqrt{(1+\delta_{ab})(1+\delta_{cd})} \; , \qquad (4.3)$$

and

$$\hat{H}'_2 = \frac{1}{2} \sum_{abcd} \sum_{K,T=0,1} E_{KT}(ac,bd) [\hat{\rho}_{KT}(i) \times \hat{\rho}_{KT}(j)]^{J=0} \; . \qquad (4.4)$$

Here, we define $\hat{\rho}_{KMT}$ as

$$\hat{\rho}_{K\,MT} = \hat{\rho}_{K\,Mp} + (-1)^T \hat{\rho}_{K\,Mn} \; , \qquad (4.5)$$

and the E_{KT} are given by

$$E_{KT=0}(ac,bd) = (-1)^{j_b+j_c}\sum_J(-1)^J(2J+1)\begin{Bmatrix} j_a & j_b & J \\ j_d & j_c & K \end{Bmatrix}\sqrt{(1+\delta_{ab})(1+\delta_{cd})}$$
$$\times \quad \tfrac{1}{2}\left[V^N_{JT=1}(ab,cd)+\tfrac{1}{2}(V^A_{JT=0}(ab,cd)-V^S_{JT=1}(ab,cd))\right] \ , \quad (4.6)$$

$$E_{KT=1}(ac,bd) = -(-1)^{j_b+j_c}\sum_J(-1)^J(2J+1)\begin{Bmatrix} j_a & j_b & J \\ j_d & j_c & K \end{Bmatrix}\sqrt{(1+\delta_{ab})(1+\delta_{cd})}$$
$$\times \quad \tfrac{1}{4}\left(V^A_{JT=0}(ab,cd)-V^S_{JT=1}(ab,cd)\right). \quad (4.7)$$

Note that $E_{KT=0}(ac,bd) - E_{KT=1}(ac,bd)$ is an invariant related only to the physical part of the interactions, $(V^A_{JT=1} + V^A_{JT=0})$. We can choose all $E_{KT=1}$ to be zero in the above (by setting $V^S_{JT=1} = V^A_{JT=0}$) leaving $E_{KT=0}$ completely determined by the physical matrix elements. In that case, we can halve the number of fields to be integrated.

If we now diagonalize the $E_{KT}(i,j)$ as before and form the operators

$$\hat{Q}_{KMT}(\alpha) \equiv \frac{1}{\sqrt{2(1+\delta_{M0})}}(\hat{\rho}_{KMT}(\alpha)+(-1)^M\hat{\rho}_{K-MT}(\alpha)) \ , \quad (4.8a)$$
$$\hat{P}_{KMT}(\alpha) \equiv -\frac{i}{\sqrt{2(1+\delta_{M0})}}(\hat{\rho}_{KMT}(\alpha)-(-1)^M\hat{\rho}_{K-MT}(\alpha)) \ , \quad (4.8b)$$

the two-body part of the Hamiltonian can finally be written as

$$\hat{H}'_2 = \frac{1}{2}\sum_{KT}\sum_{\alpha}\lambda_{KT}(\alpha)\sum_{M\geq 0}\left(\hat{Q}^2_{K\,MT}(\alpha)+\hat{P}^2_{K\,MT}(\alpha)\right) . \quad (4.9)$$

In this decomposition, the one-body Hamiltonian $\hat{h}$ of the HS transformation does not mix protons and neutrons. We can then represent the proton and neutron wavefunctions by separate determinants, and the number of neutrons and protons will be conserved rigorously during each Monte Carlo sample. For general interactions, even if we choose nonzero $E_{KT=1}$ matrix elements, the number of fields involved is half that for a decomposition that mixes neutrons and protons, and the matrix dimension is also halved. These two factors combine to speed up the computation significantly. In this sense, an isospin formalism is more favorable, although at the cost of limiting the degrees of freedom embodied in the symmetric matrix elements V^S_j.

5 Monte Carlo quadrature and sign problems

The manipulations of the previous sections have reduced the shell model to quadrature. That is, thermodynamic expectation values are given as the ratio of two multidimensional integrals over the auxiliary fields. The dimension D of these integrals is of order $N_s^2 N_t$, which can exceed 10^5 for the problems of

interest. Monte Carlo methods are the only practical means of evaluating such integrals. A more general discussion may be found in Ref. (44).

Monte Carlo quadrature can be a very efficient way of evaluating integrals of high dimension. The name "Monte Carlo" arises from the random or "chance" character of the method and the famous casino in Monaco. The essential idea is not to evaluate the integrand at every one of a large number of quadrature points, but rather at only a representative random sampling of fields. This is analogous to predicting the results of an election on the basis of a poll of a small number of voters.

To apply Monte Carlo quadrature to the shell model (i.e., expressions such as (3.14)), the weight function W_σ must be real and non-negative. While the properties of W clearly depend upon the interaction and decomposition used, these conditions are not satisfied for the natural decompositions of most realistic Hamiltonians. However, a broad class of schematic interactions and all realistic interactions satisfy these conditions closely enough (or, occasionally, exactly) so that Monte Carlo quadrature can be used.

Although we have briefly alluded to "sign problems" in some of the previous chapters, virtually all of our discussion has been based on the premise that the weight function W_σ of Eq. (3.14) is non-negative for all field configurations σ.

Unfortunately, many of the Hamiltonians of physical interest suffer from a sign problem, in that W_σ is negative over significant fractions of the integration volume. To understand the implications of this, let us rewrite Eq. (3.14) as

$$\langle \hat{\Omega} \rangle = \int d^D\sigma P_\sigma \Phi_\sigma \Omega_\sigma \ , \tag{5.1}$$

where

$$P_\sigma = \frac{\mid W_\sigma \mid}{\int d^D\sigma \mid W_\sigma \mid \Phi_\sigma} \ ,$$

and $\Phi_\sigma = W_\sigma / \mid W_\sigma \mid$ is the sign of the real part of W_σ. (Note that since the partition function is real, we can neglect the imaginary part.) Since $\mid W_\sigma \mid$ is non-negative by definition, we can interpret it, suitably normalized, as a probability density, so that upon rewriting (5.1) as

$$\langle \hat{\Omega} \rangle = \frac{\int d\sigma \mid W_\sigma \mid \Phi_\sigma \Omega_\sigma}{\int d\sigma \mid W_\sigma \mid \Phi_\sigma} = \frac{\langle \Phi \hat{\Omega} \rangle}{\langle \Phi \rangle} \ , \tag{5.2}$$

we can think of the observable as a ratio in which the numerator and denominator can be separately evaluated by Monte Carlo quadrature (49). Leaving aside the issue of correlations between estimates of these two quantities (they can always be evaluated using separate Metropolis walks), the fractional variance of $\langle \hat{\Omega} \rangle$ will be

$$\frac{\sigma_\Omega}{\langle \hat{\Omega} \rangle} = \sqrt{\frac{\langle \hat{\Omega}^2 \rangle}{\langle \Phi \hat{\Omega} \rangle^2} + \frac{1}{\langle \Phi \rangle^2} - 2} \ , \tag{5.3}$$

which becomes unacceptably large as the average sign $\langle \Phi \rangle$ approaches zero. The average sign of the weight thus determines the feasibility of naive MC quadrature. Only a handful of interacting electron systems are known to give rise to a positive-definite path integral (29): the one-dimensional Hubbard model, the half-filled Hubbard model, and the attractive Hubbard model at any dimension and filling.

For the most general case, we must have a deeper understanding of the sign problem. We rewrite the canonical expectation value of an observable $\hat{\Omega}$ as

$$\langle \hat{\Omega} \rangle \equiv \frac{\mathrm{Tr}\,(\hat{\Omega} e^{-\beta \hat{H}})}{\mathrm{Tr}\,(e^{-\beta \hat{H}})} \approx \frac{\int D\sigma W_\sigma \Phi_\sigma \Omega_\sigma}{\int D\sigma W_\sigma \Phi_\sigma} , \tag{5.4}$$

where in the spirit of Eq. (5.1,5.2) we have introduced a positive-definite weight

$$W_\sigma = G_\sigma \mid \mathrm{Tr}_A \hat{U}_\sigma \mid , \tag{5.5}$$

and the Monte Carlo sign

$$\Phi_\sigma = \frac{\mathrm{Tr}_A \hat{U}_\sigma}{\mid \mathrm{Tr}_A \hat{U}_\sigma \mid} . \tag{5.6}$$

The sign problem arises because the one-body partition function $\mathrm{Tr}_A \hat{U}_\sigma$ is not necessarily positive, so that the Monte Carlo uncertainty in the denominator of Eq. (5.2) (the W-weighted average sign, $\langle \Phi \rangle$) can become comparable to or larger than $\langle \Phi \rangle$ itself. In most cases $\langle \Phi \rangle$ decreases exponentially with β or with the number of time slices (47).

An important class of interactions (pairing+quadrupole) free from the sign problem (i.e., $\Phi_\sigma \equiv 1$) was found in Ref. (24). These are realized when $V_\alpha \leq 0$ for all α in Eq. (3.11). For an arbitrary Hamiltonian, we are not guaranteed that all $V_\alpha \leq 0$. However, we may expect that a *realistic* Hamiltonian will be dominated by terms like those of the schematic force (this is, after all, why the schematic forces were developed) so that it is, in some sense close to a Hamiltonian for which the MC is directly applicable. Thus, the "practical solution" to the sign problem presented in Ref. (26) is based on an extrapolation of observables calculated for a "nearby" family of Hamiltonians whose integrands have a positive sign. Success depends crucially upon the degree of extrapolation required. Empirically, one finds that, for all of the many realistic interactions tested in the *sd*- and *pf*-shells, the extrapolation required is modest, amounting to a factor-of-two variation in the isovector monopole pairing strength.

Based on the above observation, it is possible to decompose $\hat{H}$ in (3.11) into its "good" and "bad" parts, $\hat{H} = \hat{H}_G + \hat{H}_B$, with

$$\begin{aligned} \hat{H}_G &= \sum_\alpha (\epsilon_\alpha^* \hat{\bar{O}}_\alpha + \epsilon_\alpha \hat{O}_\alpha) + \frac{1}{2} \sum_{V_\alpha < 0} V_\alpha \left\{ \hat{O}_\alpha, \hat{\bar{O}}_\alpha \right\} \\ \hat{H}_B &= \frac{1}{2} \sum_{V_\alpha > 0} V_\alpha \left\{ \hat{O}_\alpha, \hat{\bar{O}}_\alpha \right\} . \end{aligned} \tag{5.7}$$

The "good" Hamiltonian $\hat{H}_G$ includes, in addition to the one-body terms, all the two-body interactions with $V_\alpha \leq 0$, while the "bad" Hamiltonian $\hat{H}_B$ contains all interactions with $V_\alpha > 0$. By construction, calculations with $\hat{H}_G$ alone have $\Phi_\sigma \equiv 1$ and are thus free of the sign problem.

We define a family of Hamiltonians $\hat{H}_g$ that depend on a continuous real parameter g as $\hat{H}_g = f(g)\hat{H}_G + g\hat{H}_B$, so that $\hat{H}_{g=1} = \hat{H}$, and $f(g)$ is a function with $f(1) = 1$ and $f(g < 0) > 0$ that can be chosen to make the extrapolations less severe. (In practical applications $f(g) = 1-(1-g)/\chi$ with $\chi \approx 4$ has been found to be a good choice.) If the V_α that are large in magnitude are "good," we expect that $\hat{H}_{g=0} = \hat{H}_G$ is a reasonable starting point for the calculation of an observable $\langle\hat{\Omega}\rangle$. One might then hope to calculate $\langle\hat{\Omega}\rangle_g = \mathrm{Tr}\,(\hat{\Omega}e^{-\beta\hat{H}_g})/\mathrm{Tr}\,(e^{-\beta\hat{H}_g})$ for small $g > 0$ and then to extrapolate to $g = 1$, but typically $\langle\Phi\rangle$ collapses even for small positive g. However, it is evident from our construction that $\hat{H}_g$ is characterized by $\Phi_\sigma \equiv 1$ for any $g \leq 0$, since all the "bad" $V_\alpha(> 0)$ are replaced by "good" $gV_\alpha < 0$. We can therefore calculate $\langle\hat{\Omega}\rangle_g$ for any $g \leq 0$ by a Monte Carlo sampling that is free of the sign problem. If $\langle\hat{\Omega}\rangle_g$ is a smooth function of g, it should then be possible to extrapolate to $g = 1$ (i.e., to the original Hamiltonian) from $g \leq 0$. We emphasize that $g = 0$ is not expected to be a singular point of $\langle\hat{\Omega}\rangle_g$; it is special only in the Monte Carlo evaluation.

As described in section 4, the matrices E^π_{KT} are constructed from the two-body matrix elements $V^\pi_{JT}(ab, cd)$ of good angular momentum J, isospin T, and parity $\pi = (-1)^{l_a+l_b}$ through a Pandya transformation. For interactions that are time-reversal invariant and conserve parity, the $E^\pi_{KT}(i, j)$ (here $\pi = (-1)^{l_a+l_c}$) are real symmetric matrices that can be diagonalized by a real orthogonal transformation. The eigenvectors $\hat{\rho}_{KM}(\alpha)$ play the role of $\hat{\mathcal{O}}_\alpha$ in Eq. (3.11), and the eigenvalues $\lambda_{K\pi}(\alpha)$ are proportional to V_α. In the Condon-Shortley (51) convention $\tilde{\hat{\rho}}_{KM} = \pi(-)^{K+M}\hat{\rho}_{K-M}$ so that the "good" eigenvalues satisfy sign $[\lambda_{K\pi}(\alpha)] = \pi(-)^{K+1}$ (52).

Confidence in SMMC results requires numerical validation of the methods used. Separate issues are the validation of the SMMC formalism and algorithms, as developed in sections 3–6, and of the g-extrapolation required in calculations with realistic residual interactions. These validations have been demonstrated in detail elsewhere (25, 22).

6 Selected results

The previous sections have outlined the motivation, formalism, and implementation of Monte Carlo methods for treating the nuclear shell model. Of course, the ultimate goal of this work is to gain insight into the properties of real nuclei under a variety of conditions. In this section, we present a sampling of such results and their interpretation. The calculations presented should be viewed only as an indication of the power and potential of the method; undoubtedly, more work of this sort, abetted by ever-increasing computer power, will follow in the future.

6.1 Ground state properties of pf-shell nuclei

While complete $0\hbar\omega$ calculations can be carried out by direct diagonalization in the p- and sd-shells, the exponentially increasing number of configurations limits such studies in the next (pf) shell to only the very lightest nuclei (39, 45). SMMC techniques allow calculation of ground state observables in the full $0\hbar\omega$ model space for nuclei throughout the pf-shell. Here, we discuss a set of such calculations that use the modified KB3 interaction (19); the single-particle basis is such that $N_s = 20$ for both protons and neutrons. A more detailed description of the calculations and their results are found in Ref. (48).

These studies were performed for 28 even-even Ti, Cr, Fe, Ni, and Zn isotopes; extension to heavier nuclei is dubious because of the neglect of the $g_{9/2}$ orbital. We have used $\beta = 2$ MeV^{-1} with fixed $\Delta\beta = 1/32$ MeV^{-1}; test calculations at varying β show that the results accurately reflect the ground state properties. Some 4000-5000 independent Monte Carlo samples were taken for six equally-spaced values of g between -1 and 0, and observables were extrapolated to $g = 1$ using linear or quadratic functions, as required. We chose the parameter $\chi = 4$, as described in section 5.

Figure 6.1 shows systematic results for the mass-defects, obtained directly from $\langle \hat{H} \rangle$. The SMMC results have been corrected for the Coulomb energy, which is not included in the KB3 interaction, using (45)

$$H_{\rm Coul} = \frac{\pi(\pi-1)}{2} \cdot 0.35 - \pi\nu 0.05 + \pi \cdot 7.289 \,, \tag{6.1}$$

where π and ν are the numbers of valence protons and neutrons, respectively, and the energy is in MeV. As in Ref. (45), we have increased the calculated energy expectation values by $0.014 \cdot n(n-1)$ MeV (where $n = \pi + \nu$ is the number of valence nucleons) to correct for a "tiny" residual monopole defect in the KB3 interaction. In general, there is excellent agreement; the average error for the nuclei shown is +0.45 MeV, which agrees roughly with the internal excitation energy of a few hundred keV expected in our finite-temperature calculation.

The Gamow-Teller (GT) properties of nuclei in this region of the periodic table are crucial for supernova physics (11). These strengths are defined as

$$B(GT_{\pm}) = \langle (\sigma\tau_{\pm})^2 \rangle. \tag{6.2}$$

Note that the Ikeda sum rule, $B(\mathrm{GT}_-) - B(\mathrm{GT}_+) = 3(N-Z)$ is satisfied exactly by our calculations. In Figure 6.2, we show the calculated $B(\mathrm{GT}_+)$ for all pf-shell nuclei for which this quantity has been measured by (n,p) reactions. (For the odd nuclei ^{51}V, ^{55}Mn and ^{59}Co the SMMC calculations have been performed at $\beta = 1$ MeV^{-1} to avoid the odd-A sign problem. For even-even nuclei the GT strength calculated at this temperature is still a good approximation for the ground state value, as is shown below). Since the experimental values are normalized to measured β-decay ft values, and it is believed that the axial coupling constant is renormalized from its free value ($g_A = 1.26$) to $g_A = 1$ in nuclei (21, 45), we have multiplied all calculated results by $(1/1.26)^2$. Note

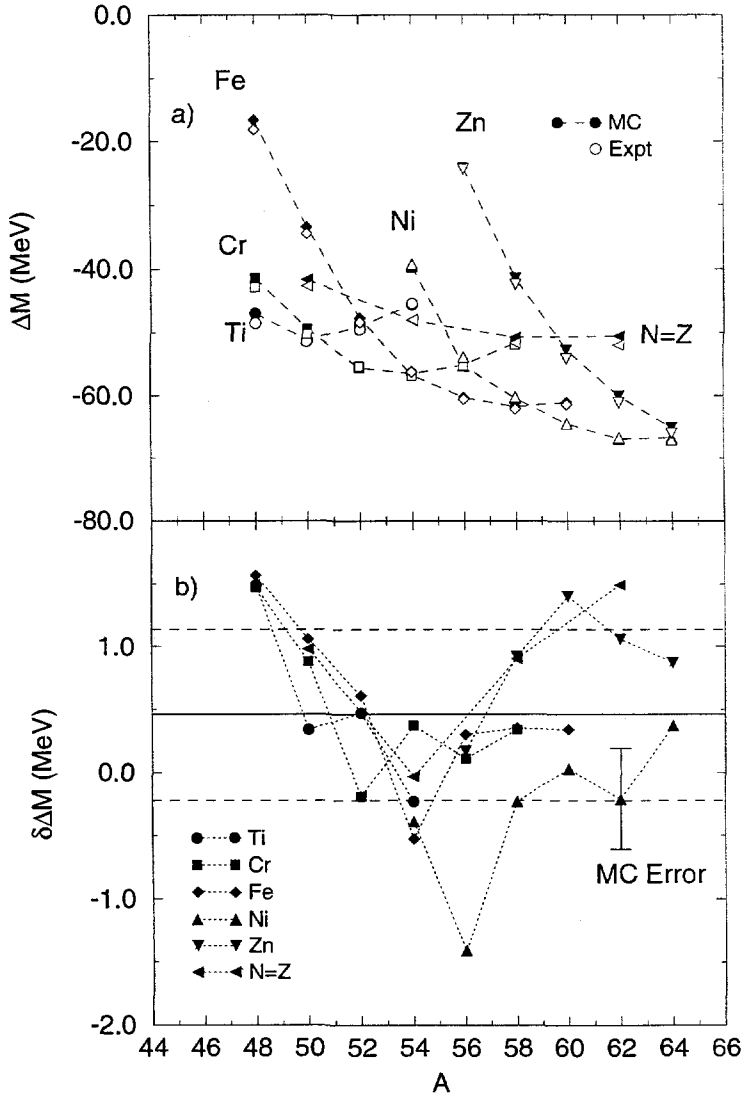

FIG 6.1. Upper panel (a): Comparison of the mass excesses ΔM as calculated within the SMMC approach with data. Lower panel (b): Discrepancy between the SMMC results for the mass excesses and the data, $\delta\Delta M$. The solid line shows the average discrepancy, 450 keV, while the dashed lines show the rms variation about this value (from 48).

that this results in generally excellent agreement between the calculations and the data. Thus, we support both the statement that g_A is quenched to 1 in nuclei and the statement that complete shell-model calculations can account for the GT strength observed experimentally. Note that the quenching of g_A in the nuclear medium is not quite understood yet. It is believed to be related either to a second-order core polarization caused by the tensor force (58) or to the screening of the Gamow-Teller operator by Δ-hole pairs (59).

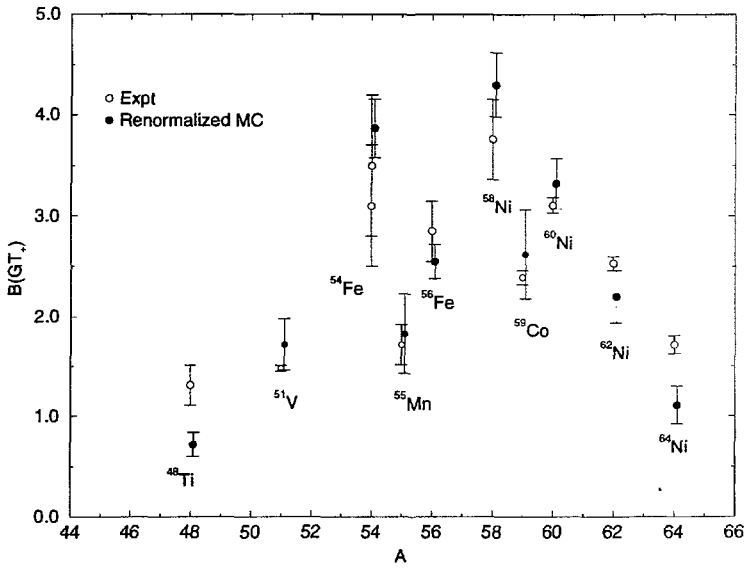

FIG 6.2. Comparison of the renormalized total Gamow-Teller strength, as calculated within the present SMMC approach, and the experimental $B(GT_+)$ values deduced from (n,p) data (53-57).

6.2 Pair structure of the nuclear ground state

Numerous phenomenological descriptions of nuclear collective motion describe the nuclear ground state and its low-lying excitations in terms of bosons. In one such model, the Interacting Boson Model (IBM), $L = 0$ (S) and $L = 2$ (D) bosons are identified with nucleon pairs having the same quantum numbers (13), and the ground state can be viewed as a condensate of such pairs. Shell model studies of the pair structure of the ground state and its variation with the number of valence nucleons can therefore shed light on the validity and microscopic foundations of these boson approaches.

To explore the pair content of the ground state in a general way, we define

proton pair creation operators

$$\hat{A}^\dagger_{J\mu}(j_a j_b) = \frac{1}{\sqrt{1+\delta_{ab}}}[a^\dagger_{j_a} \times a^\dagger_{j_b}]_{J\mu} \; . \tag{6.3}$$

These operators are boson-like in the sense that

$$[\hat{A}^\dagger_{J\mu}(j_a j_b), \hat{A}_{J\mu}(j_a j_b)] = 1 + \mathcal{O}(\hat{n}/2j+1) \; ; \tag{6.4}$$

i.e., they satisfy the expected commutation relations in the limit of an empty shell.

We construct bosons $\hat{B}^\dagger_{\alpha J\mu}$ as

$$\hat{B}^\dagger_{\alpha J\mu} = \sum_{j_a j_b} \psi_{\alpha\lambda}(j_a j_b)\hat{A}^\dagger_{\lambda\mu}(j_a j_b) \; , \tag{6.5}$$

where $\alpha = 1, 2, \ldots$ labels the particular boson and the "wave function" ψ satisfies

$$\sum_{j_a j_b} \psi^*_{\alpha J}(j_a j_b)\psi_{\beta J}(j_a j_b) = \delta_{\alpha\beta} \; . \tag{6.6}$$

(Note that ψ is independent of μ by rotational invariance.)

To find ψ and $n_{\alpha J} \equiv \sum_\mu \langle \hat{B}^\dagger_{\alpha J\mu}\hat{B}_{\alpha J\mu}\rangle$, the number of bosons of type α and multipolarity J, we compute the quantity $\sum_\mu \langle \hat{A}^\dagger_{J\mu}(j_a j_b)\hat{A}_{J\mu}(j_c j_d)\rangle$, which can be thought of as an hermitian matrix $M^J_{\alpha\alpha'}$ in the space of orbital pairs $(j_a j_b)$; its non-negative eigenvalues define the $n_{\alpha J}$ (we order them so that $n_{1J} > n_{2J} > \ldots$), while the normalized eigenvectors are the $\psi_{\alpha J}(j_a j_b)$. The index α distinguishes the various possible bosons. For example, in the complete pf-shell the square matrix M has dimension $N_J = 4$ for $J = 0$, $N_J = 10$ for $J = 1$, $N_J = 13$ for $J = 2, 3$.

It has long been anticipated that $J = 0^+$ proton-neutron correlations play an important role in the ground states of $N = Z$ nuclei. To explore these correlations, we have performed SMMC calculations of the $N = Z$ nuclei in the mass region $A = 48 - 56$. Note that for these nuclei the pair matrix in all three isovector 0^+ channels essentially exhibits only one large eigenvalue related to the $f_{7/2}$ orbital. We will use this eigenvalue as a convenient measure of the pairing strength. As the even-even $N = Z$ nuclei have isospin $T = 0$, the expectation values of $\hat{A}^\dagger\hat{A}$ are identical in all three isovector 0^+ pairing channels. This symmetry does not hold for the odd-odd $N = Z$ nuclei in this mass range, which have $T = 1$ ground states, and $\langle \hat{A}^\dagger\hat{A}\rangle$ can be different for proton-neutron pairs than for like-nucleon pairs. (The expectation values for proton pairs and neutron pairs are identical.) We find the proton-neutron pairing strength significantly larger for odd-odd $N = Z$ nuclei than in even-even nuclei, while the 0^+ proton and neutron pairing shows the opposite behavior, in both cases leading to an odd-even staggering, as displayed in Fig. 6.3. This staggering is caused by a constructive interference of the isotensor and isoscalar parts of $\hat{A}^\dagger\hat{A}$ in the odd-odd $N = Z$ nuclei, while they interfere destructively in the even-even nuclei. The isoscalar part is related to the pairing energy, and is found to be about constant for the nuclei studied here.

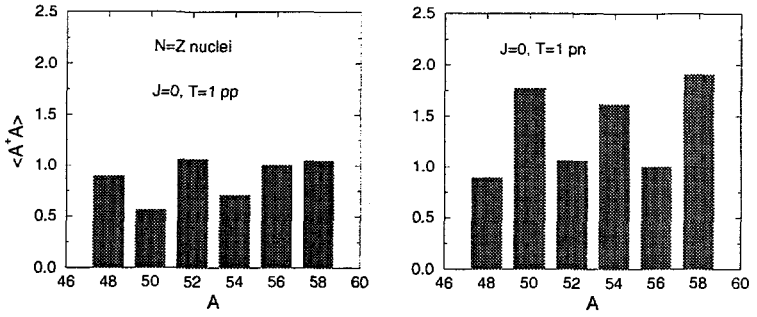

FIG 6.3. Largest eigenvalue for the various isovector 0^+ pairs in the $N = Z$ nuclei in the mass region $A = 48 - 56$.

6.3 Thermal properties of pf-shell nuclei

The properties of nuclei at finite temperatures are of considerable experimental (60, 61) and theoretical interest (62, 63). They are clearly quite important in various astrophysical scenarios. For example, electron capture on nuclei plays an essential role in the early presupernova collapse (11). In that context, it is important to know the temperature dependence of the Gamow-Teller strength.

Theoretical studies of nuclei at finite temperature have been based mainly on mean-field approaches, and thus only consider the temperature dependence of the most probable configuration in a given system. These approaches have been criticized due to their neglect of quantum and statistical fluctuations (64). The SMMC method does not suffer this defect and allows the consideration of model spaces large enough to account for the relevant nucleon-nucleon correlations at low and moderate temperatures.

We have performed SMMC calculations of the thermal properties of several even-even nuclei in the mass region $A = 50 - 60$ (65, 66). As a typical example, we discuss in the following our SMMC results for the nucleus ^{54}Fe, which is very abundant in the presupernova core of a massive star.

Our calculations include the complete set of $1p_{3/2,1/2}0f_{7/2,5/2}$ states interacting through the realistic Brown-Richter Hamiltonian (39). (SMMC calculations using the modified KB3 interaction give essentially the same results.) Some 5×10^9 configurations of the 8 valence neutrons and 6 valence protons moving in these 20 orbitals are involved in the canonical ensemble. The results presented below have been obtained with a time step of $\Delta\beta = 1/32$ MeV^{-1} using 5000–9000 independent Monte Carlo samples at seven values of the coupling constant g spaced between -1 and 0 and the value $\chi = 4$.

The calculated temperature dependence of various observables is shown in Fig. 6.4. In accord with general thermodynamic principles, the internal energy U steadily increases with increasing temperature (65). It shows an inflection point around $T \approx 1.1$ MeV, leading to a peak in the heat capacity, $C \equiv dU/dT$, whose physical origin we will discuss below. The decrease in C for $T \gtrsim 1.4$ MeV

is due to our finite model space (the Schottky effect (67)); we estimate that limitation of the model space to only the pf-shell renders our calculations of ^{54}Fe quantitatively unreliable for temperatures above this value (internal energies $U \gtrsim 15$ MeV). The same behavior is apparent in the level density parameter, $a \equiv C/2T$. The empirical value for a is $A/8$ MeV $= 6.8$ MeV^{-1} which is in good agreement with our results for $T \approx 1.1$–1.5 MeV.

We also show in Fig. 6.4 the expectation values of the BCS-like proton-proton and neutron-neutron pairing fields, $\langle \hat{\Delta}^\dagger \hat{\Delta} \rangle$. At low temperatures, the pairing fields are significantly larger than those calculated for a non-interacting Fermi gas, indicating a strong coherence in the ground state. With increasing temperature, the pairing fields decrease, and both approach the Fermi gas values for $T \approx 1.5$ MeV and follow it closely for even higher temperatures. Associated with the breaking of pairs is a dramatic increase in the moment of inertia, $I \equiv \langle J^2 \rangle / 3T$, for $T = 1.0$–1.5 MeV; this is analogous to the rapid increase in magnetic susceptibility in a superconductor. At temperatures above 1.5 MeV, I is in agreement with the rigid rotor value, $10.7\hbar^2$/MeV; at even higher temperatures it decreases linearly due to our finite model space. We note also that the Gamow-Teller total strength is relatively constant up to 2.0 MeV (not shown). We note that it is often assumed in astrophysical calculations that the GT strength is independent of temperature (68); our calculations demonstrate that this is true for the relevant temperature regime ($T < 2$ MeV).

Although the results discussed above are typical for even-even nuclei in this mass region (including the $N = Z$ nucleus ^{52}Fe), they are not for odd-odd $N = Z$ nuclei. This is illustrated in Fig. 6.5 which shows the thermal behavior of several observables for ^{50}Mn ($N = Z = 25$), calculated in a SMMC study within the complete pf-shell using the KB3 interaction. In contrast to even-even nuclei, the total Gamow-Teller strength is not constant at low temperatures, but increases by about 50% between $T = 0.4$ MeV and 1 MeV. The $B(M1)$ strength decreases significantly in the same temperature interval, while for even-even nuclei, it increases steadily. A closer inspection of the isovector $J = 0$ and isoscalar $J = 1$ pairing correlations holds the key to the understanding of these differences. The $J = 0$ isovector correlations are studied using the BCS pair operators (8.6), with a similar definition for proton-neutron pairing. For the isoscalar $J = 1$ correlations, we have interpreted the trace of the pair matrix $M^{J=1}$ as an overall measure for the pairing strength,

$$P^J_{sm} = \sum_\beta \lambda^J_\beta = \sum_\alpha M^J_{\alpha\alpha}. \tag{6.7}$$

Note that at the level of the non-interacting Fermi gas, proton-proton, neutron-neutron, and proton-neutron $J = 0$ correlations are identical for $N = Z$ nuclei. However, the residual interaction breaks the symmetry between like-pair correlations and proton-neutron correlations in odd-odd $N = Z$ nuclei. As is obvious from Fig. 6.5, at low temperatures proton-neutron pairing dominates in ^{50}Mn, while pairing among like-nucleons shows only a small excess over the Fermi gas values, in strong contrast to even-even nuclei.

A striking feature of Fig. 6.5 is that the isovector proton-neutron correlations decrease strongly with temperature and have essentially vanished at $T = 1$ MeV, while the isoscalar pairing strength remains about constant in this temperature region (as it does in even-even nuclei) and greatly exceeds the Fermi gas values. We also note that the pairing between like-nucleons is roughly constant at $T < 1$ MeV. The change of importance between isovector and isoscalar proton-neutron correlations with temperature is nicely reflected in the isospin expectation value, which decreases from $< \hat{T}^2 >= 2$ at temperatures around 0.5 MeV, corresponding to the dominance of isovector correlations, to $< \hat{T}^2 >= 0$ at temperature $T = 1$ MeV, when isoscalar proton-neutron correlations are most important. The low-temperature behavior of the Gamow-Teller and $B(M1)$ strength is related to the fading of the isoscalar proton-neutron correlations. For example, the Gamow-Teller strength increases as transitions between the same orbital (mainly $f_{7/2}$) are less quenched by weaker isovector proton-neutron correlations.

6.4 Electron capture and presupernova collapse

The core of a massive star at the end of hydrostatic burning is stabilized by electron degeneracy pressure as long as its mass does not exceed the appropriate Chandrasekhar mass M_{CH}. If the core mass exceeds M_{CH}, electrons are captured by nuclei (11) to avoid a violation of the Pauli principle:

$$e^- + (Z, A) \rightarrow (Z - 1, A) + \nu_e \,. \tag{6.8}$$

The neutrinos can still escape from the core, carrying away energy. This is accompanied by a loss of pressure and the collapse is accelerated.

For many of the nuclei that determine the electron capture rate in the early stage of the presupernova (68), Gamow-Teller (GT) transitions contribute significantly to the electron capture rate. Due to insufficient experimental information, the GT_+ transition rates have so far been treated only qualitatively in presupernova collapse simulations, assuming the GT_+ strength to reside in a single resonance, whose energy relative to the daughter ground state has been parametrized phenomenologically (69); the total GT_+ strength has been taken from the single particle model. Recent (n, p) experiments (53-57), however, show that the GT_+ strength is fragmented over many states, while the total strength is significantly quenched compared to the single particle model (see section 8.1). (A recent update of the GT_+ rates for use in supernova simulations assumed a constant quenching factor of 2 (68).)

In a series of truncated shell model calculations, Aufderheide and collaborators have demonstrated that a strong phase space dependence makes the Gamow-Teller contributions to the presupernova electron capture rates more sensitive to the strength *distribution* in the daughter nucleus than to the total strength (70). In this work it also became apparent that complete $0\hbar\omega$ studies of the GT_+ strength distribution are desirable. Such studies are now possible using the SMMC approach.

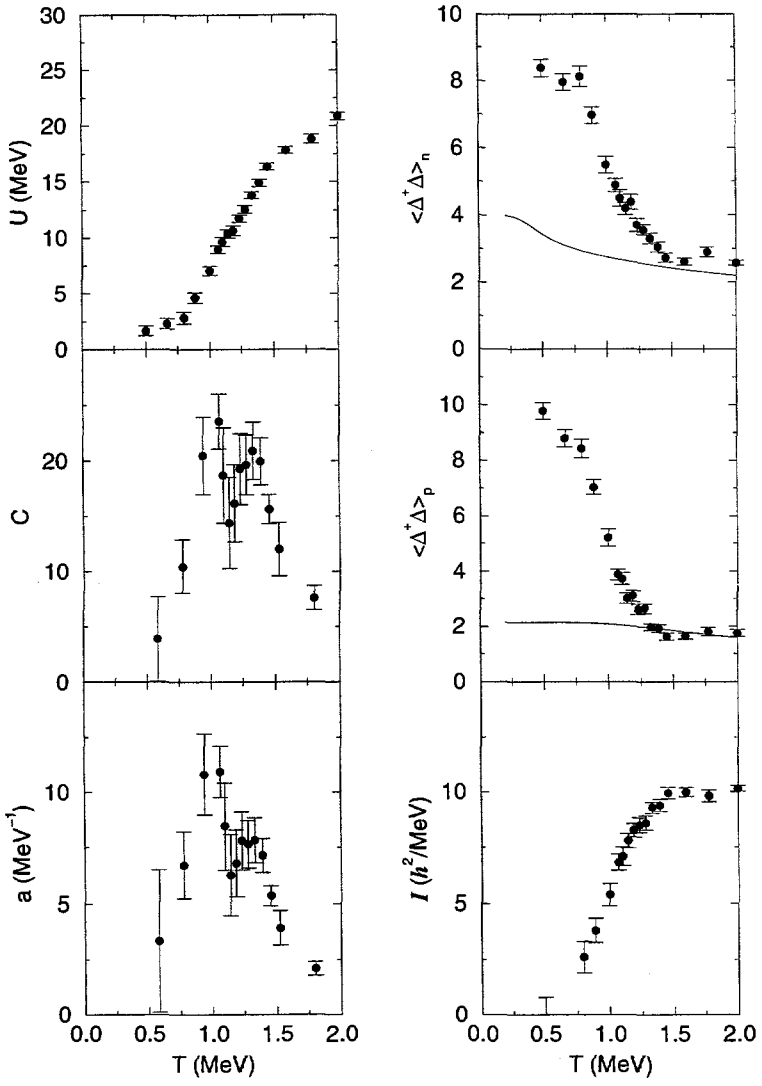

FIG 6.4. Temperature dependence of various observables in ^{54}Fe. Monte Carlo points with statistical errors are shown at each temperature T. In the left-hand column, the internal energy, U, is calculated as $\langle \hat{H} \rangle - E_0$, where $\hat{H}$ is the many-body Hamiltonian and E_0 the ground state energy. The heat capacity C is calculated by a finite-difference approximation to dU/dT, after $U(T)$ has been subjected to a three-point smoothing, and the level density parameter is $a \equiv C/2T$. In the right-hand column, we show the expectation values of the squares of the proton and neutron BCS pairing fields. For comparison, the pairing fields calculated in an uncorrelated Fermi gas are shown by the solid curve. The moment of inertia is obtained from the expectation values of the square of the total angular momentum by $I = \beta\langle \hat{J}^2 \rangle/3$ (from 65).

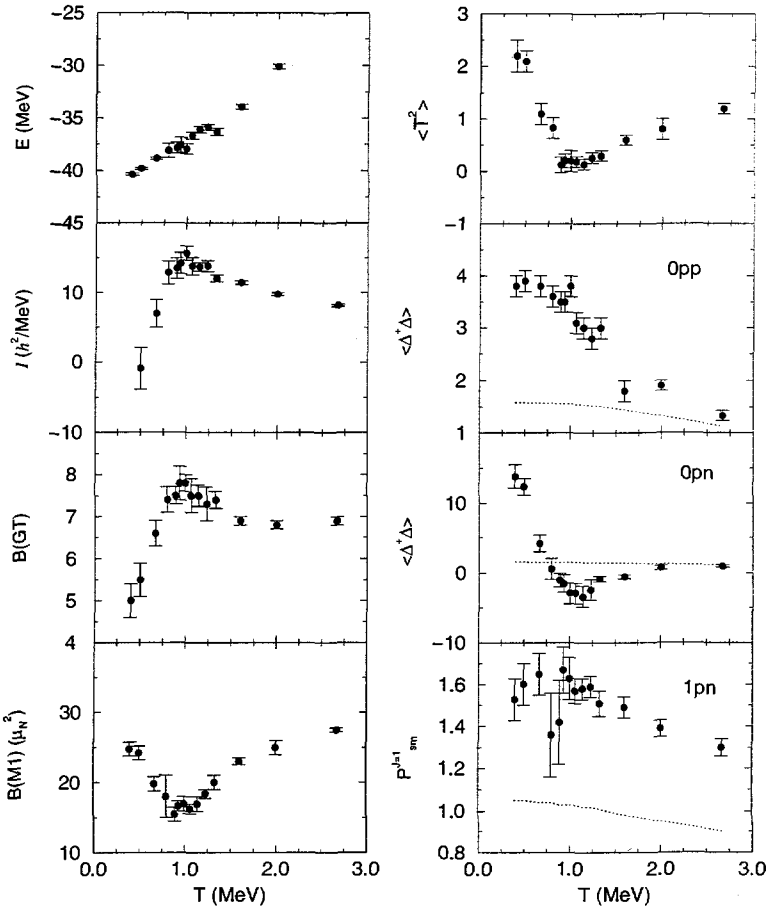

FIG 6.5 Temperature dependence of various observables in ^{50}Mn. The left panels show (from top to bottom) the total energy, the moment of inertia, the $B(M1)$ strength, and the Gamow-Teller strength, while the right panels exhibit the expectation values of the isospin operator $\langle \hat{T}^2 \rangle$, the isovector $J = 0$ proton-proton and proton-neutron BCS pairing fields, and the isoscalar $J = 1$ pairing strength, as defined in the text. For comparison, the solid lines indicate the Fermi gas values of the BCS pairing fields and $J = 1$ pairing strength.

To determine the GT_+ strength distribution, we have calculated the response function of the $\sigma\tau_+$ operator, $R_{GT}(\tau)$, as defined in Eq. (3.6). As the strength function $S_{GT}(E)$ is the inverse Laplace transform of $R_{GT}(\tau)$, we have used the Maximum Entropy technique, described in section 6.4, to extract $S_{GT}(E)$. For the default model $m(E)$ in (6.21) we adopted a Gaussian whose centroid is given by the slope of $\ln R_{GT}(\tau)$ at small τ and whose width is 2 MeV.

As first examples we have studied several nuclei (^{51}V, ^{54,56}Fe, ^{58,60,62}Ni, and

^{59}Co), for which the Gamow-Teller strength distribution in the daughter nucleus is known from (n,p) experiments (53-57). Note that the electron capture by these nuclei, however, plays only a minor role in the presupernova collapse. As SMMC calculates the strength function within the parent nucleus, the results have been shifted using the experimental Q-value. The Coulomb correction has been performed using Eq. (8.1). For all nuclei, the SMMC approach calculates the centroid and width of the strength distribution in good agreement with data. (Following Ref. (46) the calculated strength distributions have been folded with Gaussians of width 1.77 MeV to account for the experimental resolution.) Fig. 6.6 shows the response function $R_{GT}(\tau)$ for ^{54}Fe and ^{59}Co and compares the extracted GT_+ strength distribution with data. (As discussed in sections 8.1 and 8.5, the Gamow-Teller operator has been renormalized by the factor 0.77). The centroid of the GT_+ strength distributions is found to be nearly independent of temperature (calculations for odd nuclei could be performed only in the temperature range $T = 0.8 - 1.2$ MeV), while its width increases with temperature. Calculations of the Gamow-Teller contribution to electron capture rates in presupernova conditions are under way.

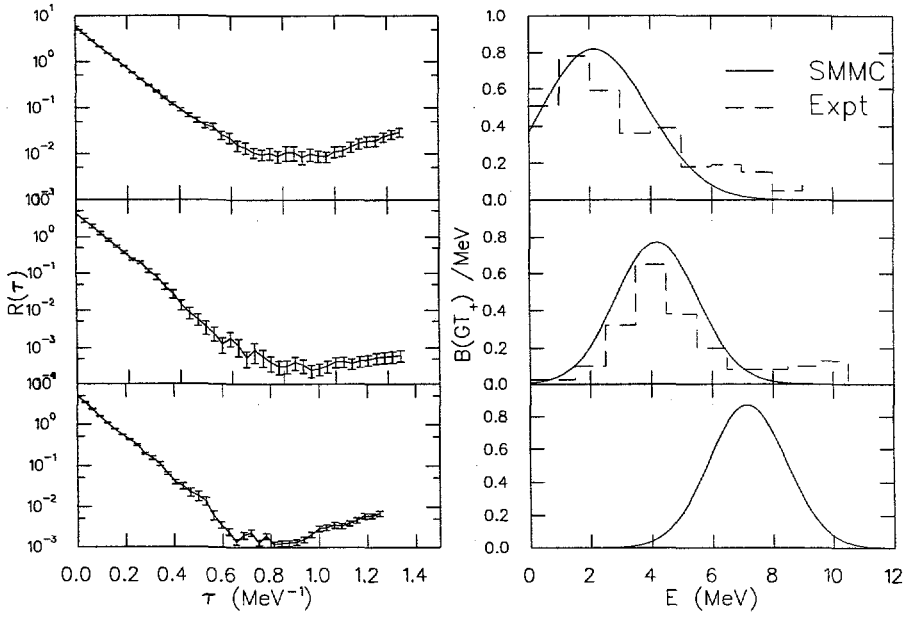

FIG 6.6. SMMC GT_+ response functions (left side) and GT_+ strength distributions (right side) for ^{54}Fe (upper panel), ^{59}Co (middle panel), and ^{55}Co (lower panel). The energies refer to the daughter nuclei. The dashed histograms show the experimental strength distribution as extracted from (n,p) data (54).

6.5 γ-soft nuclei

Nuclei with mass number $100 \leq A \leq 140$ are believed to have large shape fluctuations in their ground states. Associated with this softness are spectra with an approximate $O(5)$ symmetry and bands with energy spacings intermediate between rotational and vibrational. In the geometrical model these nuclei are described by potential energy surfaces with a minimum at $\beta \neq 0$ but independent of γ (72). Some of these nuclei have been described in terms of a quartic five-dimensional oscillator (73). In the Interacting Boson Model (IBM) they are described by an $O(6)$ dynamical symmetry (13, 74, 75). In the following we review the first fully microscopic calculations for soft nuclei with $100 \leq A \leq 140$ (76).

For the two-body interaction we used a monopole ($J = 0$) plus quadrupole ($J = 2$) force (77), supplemented by a collective quadrupole interaction:

$$\hat{H}_2 = -\sum_{\lambda\mu} \frac{\pi g_\lambda}{2\lambda+1} \hat{P}^\dagger_{\lambda\mu} \hat{P}_{\lambda\mu} - \frac{1}{2}\chi : \sum_\mu (-)^\mu \hat{Q}_\mu \hat{Q}_{-\mu} : , \tag{6.9}$$

where :: denotes normal ordering. The single particle energies and the other parameters were determined as described in Ref. (76).

In order to obtain a more detailed picture of the deformation, we examine the components of the quadrupole operator $\hat{Q}_\mu = r^2 Y^*_{2\mu}$. Note, however, that due to rotational invariance of the uncranked Hamiltonian, the expectation value of any component $\hat{Q}_\mu$ is expected to vanish. On the other hand, there is an intrinsic frame for each Monte Carlo sample, in which it is possible to compute the three non-zero components Q'_0, Q'_2, and Q'_{-2} (the prime is used to denote the intrinsic frame). The intrinsic quadrupole moments can then be related to the standard deformation coordinates β and γ (2, 25). The task remains to compute the quadrupole moments in the intrinsic frame for each Monte Carlo sample. This is accomplished by computing and diagonalizing the expectation value of the cartesian quadrupole tensor $Q_{ij} = 3x_i x_j - \delta_{ij} r^2$ for each Monte Carlo sample. From the three eigenvalues, it is straightforward to determine the deformation parameters as in Ref. (71).

We begin discussion of our results with the probability distribution of the quadrupole moment. These contour plots show the free energy $F(\beta, \gamma)$, obtained from the shape probability distribution, $P(\beta, \gamma)$, by

$$F(\beta, \gamma) = -T \ln \frac{\mathcal{P}(\beta, \gamma)}{\beta^3 \sin 3\gamma} \tag{6.10}$$

where the $\beta^3 \sin 3\gamma$ is the metric in the usual deformation coordinates; $\mathcal{P}$ was obtained simply by binning the Monte Carlo samples in the $\beta - \gamma$ plane. The calculation of the shape distributions included the quantum-mechanical fluctuations through the variance of the $\hat{Q}$ operator for each sample, $\Delta^2_\sigma = \mathrm{Tr}(\hat{Q}^2 \hat{U}_\sigma)/\mathrm{Tr}(\hat{U}_\sigma) - \langle \hat{Q} \rangle^2_\sigma$. The shape distribution $P(\beta, \gamma)$ can be converted to a free energy surface as described by Eq. (8.19).

The shape distributions of ^{128}Te and ^{124}Xe are shown in Fig. 6.7 at different temperatures. These nuclei are clearly γ-soft, with energy minima at $\beta \sim 0.06$ and $\beta \sim 0.15$, respectively. Energy surfaces calculated with Strutinsky-BCS using a deformed Woods-Saxon potential (78) also indicate γ-softness with values of β comparable to the SMMC values. These calculations predict for ^{124}Xe a prolate minimum with $\beta \approx 0.20$ which is lower than the spherical configuration by 1.7 MeV but is only 0.3 MeV below the oblate saddle point, and for ^{128}Te a shallow oblate minimum with $\beta \approx 0.03$. These γ-soft surfaces are similar to those obtained in the $O(6)$ symmetry of the IBM, or more generally when the Hamiltonian has mixed $U(5)$ and $O(6)$ symmetries but a common $O(5)$ symmetry. In the Bohr Hamiltonian, an $O(5)$ symmetry occurs when the collective potential energy depends only on β (72). The same results are consistent with a potential energy $V(\beta)$ that has a quartic anharmonicity (73), but with a negative quadratic term that leads to a minimum at finite β.

The total E2 strengths were estimated from $\langle \hat{Q}^2 \rangle$ where $\hat{Q} = e_p \hat{Q}_p + e_n \hat{Q}_n$ is the electric quadrupole operator with effective charges of $e_p = 1.5e$ and $e_n = 0.5e$, and $B(E2; 0_1^+ \rightarrow 2_1^+)$ determined by assuming that most of the strength is in the 2_1^+ state. Values for $B(E2; 0_1^+ \rightarrow 2_1^+)$ of 663 ± 10, 2106 ± 15, and 5491 ± 36 $e^2\text{fm}^4$ were found, to be compared with the experimental values (79) of 1164, 3910, and 9103 $e^2\text{fm}^4$ for ^{124}Sn, ^{128}Te and ^{124}Xe, respectively. Thus, the SMMC calculations reproduce the correct qualitative trend. The 2_1^+ excitation energies were also calculated from the E2 response function. The values of 1.12 ± 0.02, 0.96 ± 0.02 and 0.52 ± 0.01 MeV are in close agreement with the experimental values of 1.2, 0.8 and 0.6 MeV for ^{124}Sn, ^{128}Te and ^{124}Xe, respectively.

The total number of J-pairs ($n_J = \sum_\alpha n_{\alpha J}$) in the various pairing channels was also calculated. Since the number of neutrons in ^{124}Xe is larger than the mid-shell value, they are treated as holes. For $J = 0$ and $J = 2$ one can compare the largest $n_{\alpha J}$ with the number of s and d bosons obtained from the $O(6)$ limit of the IBM. For ^{124}Xe the SMMC (IBM) results in the proton-proton pairing channel are 0.85 (1.22) s ($J = 0$) pairs, and 0.76 (0.78) d ($J = 2$) pairs, while in the neutron-neutron channel we find 1.76 (3.67) s pairs and 2.14 (2.33) d pairs. For the protons the SMMC d to s pair ratio 0.89 is close to its $O(6)$ value of 0.64. However, the same ratio for the neutrons, 1.21, is intermediate between $O(6)$ and $SU(3)$ (where its value is 1.64) and is consistent with the neutrons filling the middle of the shell. The total numbers of s and d pairs – 1.61 proton pairs and 3.8 neutron (hole) pairs – are below the IBM values of 2 and 6, respectively.

6.6 Double-beta decay

The second-order weak process $(Z, A) \rightarrow (Z+2, A) + 2e^- + 2\bar{\nu}_e$ is an important "background" to searches for the lepton number-violating neutrinoless mode, $(Z, A) \rightarrow (Z+2, A)$. The calculation of the nuclear matrix element for these two processes is a challenging problem in nuclear structure, and has been done in a full pf model space for only the lightest of several candidates, ^{48}Ca. P.B.

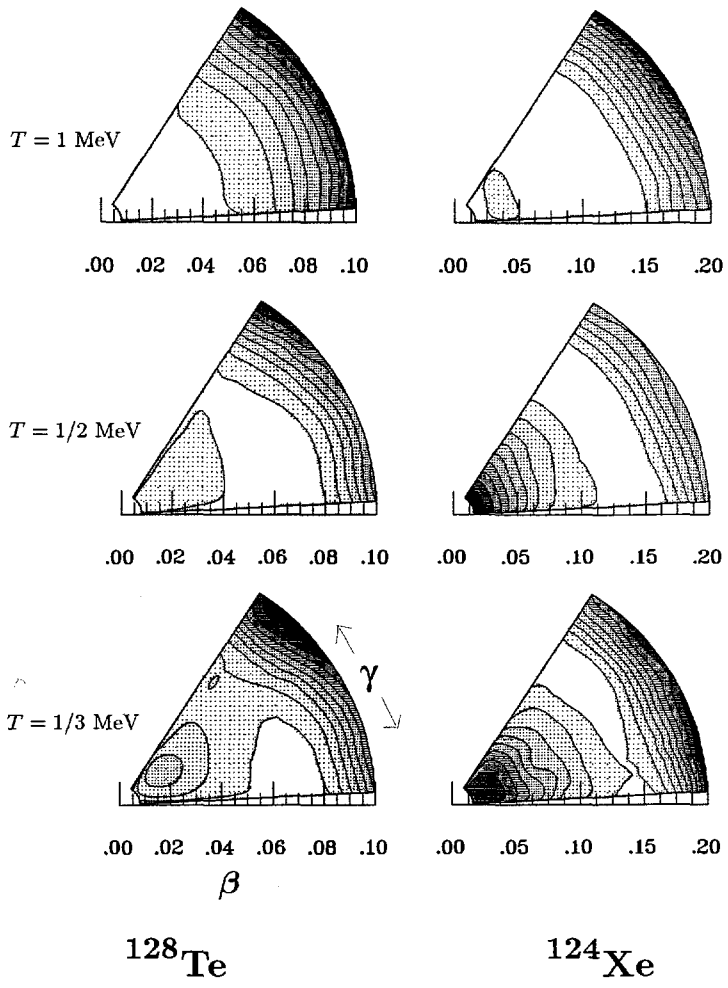

FIG 6.7. Contours of the free energy (as described in the text) in the polar-coordinate $\beta - \gamma$ plane for ^{128}Te and ^{124}Xe. Contours are shown at 0.3 MeV intervals, with lighter shades indicating the more probable nuclear shapes (from (76)).

Radha *et al.* have performed first Monte Carlo calculations of the 2ν $\beta\beta$ matrix elements in very large model spaces (80).

In two-neutrino double β-decay, the nuclear matrix element of interest is

$$M^{2\nu} \equiv \sum_m \frac{\langle f_0|\hat{\mathbf{G}}|m\rangle \cdot \langle m|\hat{\mathbf{G}}|i_0\rangle}{E_m - \Omega} , \tag{6.11}$$

where $|i_0\rangle$ and $|f_0\rangle$ are the 0^+ ground states of the initial and final even-even nuclei, and $|m\rangle$ is a 1^+ state of the intermediate odd-odd nucleus; the sum is over all such states. In this expression, $\hat{\mathbf{G}} = \sigma\tau_-$ is the Gamow-Teller operator for β^--decay (i.e., that which changes a neutron into a proton) and $\Omega = (E_{i_0} + E_{f_0})/2$. A common approximation to $M^{2\nu}$ is the closure value,

$$M^{2\nu} = \frac{M_c}{\bar{E}} \tag{6.12}$$

where $\bar{E}$ is an average energy dominator and

$$M_c \equiv \sum_m \langle f_0|\hat{\mathbf{G}}|m\rangle\langle m|\hat{\mathbf{G}}|i_0\rangle = \langle f_0|\hat{\mathbf{G}}\cdot\hat{\mathbf{G}}|i_0\rangle\ . \tag{6.13}$$

SMMC methods can be used to calculate both M_c and $M^{2\nu}$. To do so, consider the function

$$\begin{aligned}\phi(\tau,\tau') &= \langle e^{\hat{H}(\tau+\tau')}\hat{\mathbf{G}}^\dagger\cdot\hat{\mathbf{G}}^\dagger e^{-\hat{H}\tau}\hat{\mathbf{G}}e^{-\hat{H}\tau'}\hat{\mathbf{G}}\rangle \\ &= \frac{1}{Z}\mathrm{Tr}_A\left[e^{-(\beta-\tau-\tau')\hat{H}}\hat{\mathbf{G}}^\dagger\cdot\hat{\mathbf{G}}^\dagger e^{-\tau\hat{H}}\hat{\mathbf{G}}e^{-\tau'\hat{H}}\hat{\mathbf{G}}\right]\ ,\end{aligned} \tag{6.14}$$

where $Z = \mathrm{Tr}_A\, e^{-\beta\hat{H}}$ is the partition function for the initial nucleus, $\hat{H}$ is the many-body Hamiltonian, and the trace is over all states of the initial nucleus. The quantities $(\beta-\tau-\tau')$ and τ play the role of the inverse temperature in the parent and daughter nucleus respectively. A spectral expansion of ϕ shows that large values of these parameters guarantee cooling to the parent and daughter ground states. In these limits, we note that $\phi(\tau,\tau'=0)$ approaches $e^{-\tau Q}|M_c|^2$, where $Q = E_i^0 - E_f^0$ is the energy release, so that a calculation of $\phi(\tau,0)$ leads directly to the closure matrix element. If we then define

$$\eta(T,\tau) \equiv \int_0^T d\tau'\phi(\tau,\tau')e^{-\tau' Q/2}, \tag{6.15}$$

and

$$M^{2\nu}(T,\tau) \equiv \frac{\eta(T,\tau)M_c^*}{\phi(\tau,0)}, \tag{6.16}$$

it is easy to see that in the limit of large τ, $(\beta-\tau-\tau')$, and T, $M^{2\nu}(T,\tau)$ becomes independent of these parameters and is equal to the matrix element in Eq. (8.23).

In the first applications, Radha *et al.* calculated the 2ν matrix elements for ^{48}Ca and ^{76}Ge (80). The first nucleus allowed a benchmarking of the SMMC method against direct diagonalization. A large-basis shell model calculation for ^{76}Ge has long been waited for, as ^{76}Ge is one of the few nuclei where the $2\nu\beta\beta$ decay has been precisely measured and the best limits on the 0ν decay mode have been established (81, 82, 83).

The SMMC calculation for ^{48}Ca was performed for the complete pf shell using the KB3 interaction and compared to a direct diagonalization using an implementation of the Lanczos algorithm (80). We found good agreement between the two methods.

To monitor the possible uncertainty related to the g-extrapolation in the calculation of the 2ν matrix element for ^{76}Ge, SMMC studies have been performed for two quite different families of sign-problem-free Hamiltonians ($\chi = \infty$ and $\chi = 4$). The calculation comprises the complete $(0f_{5/2}, 1p, 0g_{9/2})$ model space, which is significantly larger than in previous shell model studies (84). The adopted effective interaction is based on the Paris potential and has been constructed for this model space using the Q-box method developed by Kuo (85).

As is shown in Fig. 6.8, upon linear extrapolation both families of Hamiltonians predict a consistent value for the 2ν matrix element of ^{76}Ge. The results $M^{2\nu} = 0.12 \pm 0.07$ and $M^{2\nu} = 0.12 \pm 0.06$ are only slightly lower than the experimental values ($M^{2\nu} = 0.22 \pm 0.01$, (83)). This comparison, however, should not be overinterpreted yet, as the detailed reliability of the effective interaction is still to be checked.

It is interesting that the closure matrix element found in the SMMC calculation and the average energy denominator ($M_c = -0.36 \pm 0.37$, $\bar{E} = -3.0 \pm 3.3$ MeV and $M_c = 0.08 \pm 0.17$, $\bar{E} = 0.57 \pm 1.26$ MeV for the two families of Hamiltonians with $\chi = \infty$ and $\chi = 4$, respecitvely) are both significantly smaller than had been assumed previously. This is confirmed by a recent truncated diagonalization study (86).

7 Prospects

We have presented in section 8 a sampling of results from SMMC calculations. These demonstrate both the power and limitations of the methods and the physical insights they offer. SMMC calculations, while not a panacea, clearly have certain advantages over conventional shell model approaches, particularly for properties of ground states or thermal ensembles. Of the results discussed in this review, the most significant bear on the quenching of GT strength, the pairing structure, and nuclear shapes. Many of the first applications of the SMMC approach have significant bearing on astrophysical questions.

With respect to the technical aspects of these calculations, we note the following.

- SMMC methods are computationally intensive. However, computing power is becoming both less expensive and more widely available at an astonishing rate. It is a great advantage that these calculations can efficiently exploit loosely connected "farms" of workstation-class machines.
- A number of interesting physics questions require multi-shell model spaces. Among these are the origin of the apparent renormalization of $g_A = 1$ in Gamow-Teller transitions, strengths of first-forbidden weak operators, the

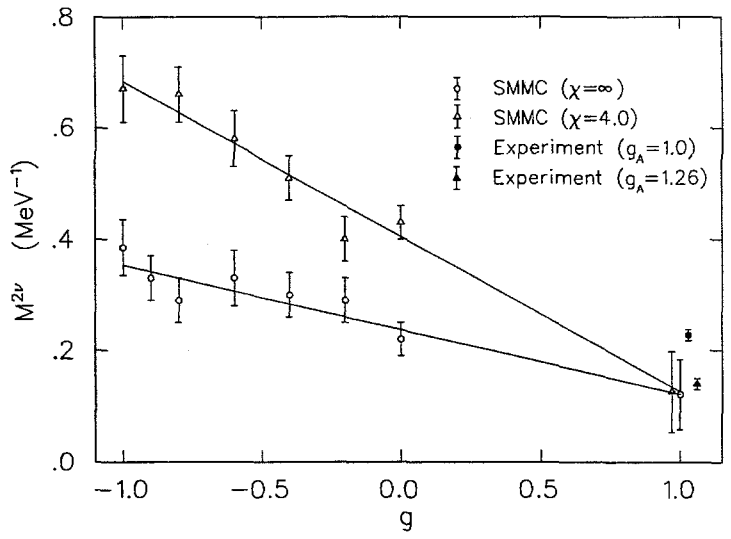

FIG 6.8. The 2ν matrix element for ^{76}Ge calculated within SMMC studies based on two families of Hamiltonians which are free of sign problems. The physical values are obtained by linear extrapolation to $g = 1$. The experimental value for this matrix element (83) is indicated by the diamond (from 80).

properties of the giant dipole resonance, and nuclear behavior at temperatures above 1.5 MeV. Preliminary SMMC studies offer circumstantial evidence that center-of-mass (CM) motion is not a significant concern for some of the operators of interest. This is not too surprising at finite temperature, since the CM is only three degrees of freedom (far fewer than the internal dynamics).

- We lack the capability to treat odd-A or odd-odd $N \neq Z$ systems at temperatures below ~800 keV, because of "sign" problems in the Monte Carlo sampling. However, meaningful results are possible at modest temperatures for such nuclei, as exemplified by the ^{51}V, ^{55}Mn, and ^{59}Co calculations in section 8.1. Similar problems prevent spin projection, which would enable yrast spectroscopy.

Otsuka and collaborators (87) have recently proposed a hybrid scheme whereby SMMC methods are used to select a many-body basis, which is then employed in a conventional diagonalization. The sign problems alluded to above are absent, and detailed spectroscopy is possible. Test applications to boson problems have shown some promise, although the utility for realistic fermion systems remains to be demonstrated. It is unfortunate that explicit angular momentum projection apparently plays an important role in these methods, as the numerical effort of that procedure increases strongly with the size of the model space.

Additional physics results in finite nuclei that should emerge in the future

include: more realistic electron capture rates in presupernova conditions, the double-beta decay matrix elements for candidates other than ^{76}Ge, systematic studies of rare earth nuclei at finite temperature and spin, studies to improve the effective interactions used, tests of such models as the IBM and RPA, and predictions of nuclear properties far from β-stability.

The ground state and thermal properties of nuclear matter are another intriguing application of SMMC methods. One approach is to use single particle states that are plane waves with periodic boundary conditions and a G-matrix derived from a realistic inter-nucleon interaction; the formalism and algorithms we have presented here are then directly applicable. An alternative approach is to work on a regular lattice of sites in coordinate space and employ Skyrme-like effective interactions that couple neighboring sites; the calculation is then similar to that for the Hubbard model for which special techniques must be used to handle the large, sparse matrices involved (29). Both approaches are currently being pursued.

Acknowledgements

Many people have contributed to the development and initial application of SMMC methods. These include Y. Alhassid, C. Johnson, G. Lang, W.E. Ormand, P.B. Radha, and, more recently, M.T. Ressell, P. Vogel, J. White, and D.C. Zheng. T. Kuo supplied us with effective interactions for those large model spaces that had never been treated before. We also wish to thank A. Arima, G. Bertsch, A. Brown, B. Mottelson, W. Nazarewicz, and A. Poves for useful discussions.

This work was supported by NSF grants PHY91-15574, PHY94-12818, and PHY94-20470, and by the US Department of Energy under Contract No. DE-AC05-96OR22464 managed by Lockheed Martin Energy Research Corp. DJD acknowledges an E.P. Wigner Fellowship from ORNL.

References

1. Meyer, M.G., Phys. Rev. **75** (1949) 1968; Haxel, O.J., Jensen, J.H.D., and Suess, H.E., Phys. Rev. **75** (1949) 1766
2. Bohr, A. and Mottelson B., *Nuclear Structure* (Benjamin, New York, 1969, 1975)
3. Ring, P. and Schuck, P., *The Nuclear Many-Body Problem* (Springer, New York, 1980)
4. Mosel, U., Nucl. Phys. **A583** (1995) 29c
5. Musolf, M.J., Donnelly, T.W., Dubach, J., Pollock, S.J., Kowalski, S., and Beise, E.J., Phys. Rep. **239** (1994) 1
6. Ericson, T.E.O. and Weise, W., *Pions and Nuclei* (Clarendon Press, Oxford, 1988)]
7. Frekers, D., Gill, D.R., and Speth, J., (Eds)*Physics at KAON* (Springer, Berlin, 1990)
8. Axen, D., Bryman, D., and Comyn, M. (Eds.)*The Vancouver Meeting on Particles and Fields* (World Scientific, Singapore, 1992)
9. Schwandt, P. in *Proceedings of the International Nuclear Physics Conference* (World Scientific, Singapore, 1990)
10. Osterfeld, F., Rev. Mod. Phys. **64** (1992) 491

11. Bethe, H.A., Rev. Mod. Phys. **62** (1990) 801
12. Fowler, W.A., in *Les Prix Nobel*-1983 (Almqvist and Wiksell International, Stockholm, Sweden, 1984), p. 88
13. Iachello, F. and Arima, A.,*The Interacting Boson Model* (Cambridge University Press, Cambridge, 1988)
14. Pudliner, B.S., Pandharipande, V.R., Carlson, J., and Wiringa, R.B., Phys. Rev. Lett. **74** (1995) 4396
15. Cohen, S. and Kurath, D., Nucl. Phys. **73** (1965) 1; **A141** (1970) 145; Kurath, D., Phys. Rev. **C7** (1973) 1390; Kurath, D. and Millener, D.J., Nucl. Phys. **A238** (1975) 269
16. Wildenthal, B. H., Prog. Part. Nucl. Phys. **11** (1984) 5
17. French, J.B., Halbert, E.C., McGrory, J.B., and Wong, S.S.M., Adv. Nucl. Phys. **3** (1969) 193; Halbert, E.C., McGrory, J.B., Wildenthal, B.H., and Pandya, S.P., Adv. Nucl. Phys. **4** (1971) 375
18. Schmid, K.W. and Grümmer, F., Rep. Prog. Phys. **50** (1987) 731; Donau, F., Schmid, K.W., and Fässler, A., Nucl. Phys. **A539** (1992) 403
19. Poves, A. and Zuker, A.P., Phys. Rep. **70** (1981) 235
20. Vallieres, M. and Novoselsky, A., Nucl. Phys. **A570** (1994) 345c
21. Wildenthal, B.H. in *Shell Model and Nuclear Structure: where do we stand?*. 2nd International Spring Seminar on Nuclear Physics, edited by A. Covello (World Scientific, 1988).
22. Koonin, S.E., D.J. Dean, D.J., and Langanke, K., Phys. Rep, in press.
23. Johnson, C.W., Koonin, S.E., Lang, G.H. and Ormand, W.E., Phys. Rev. Lett. **69** (1992) 3157
24. Lang, G.H., Johnson, C.W., Koonin, S.E., and Ormand, W.E., Phys. Rev. **C48** (1993) 1518
25. Ormand, W.E., Dean, D.J, Johnson, C.W., Lang, G.H., and Koonin, S.E., Phys. Rev. **C49** (1994) 1422
26. Alhassid, Y., Dean, D.J., Koonin, S.E., Lang, G.H., and Ormand, W.E., Phys. Rev. Lett. **72** (1994) 613
27. Hubbard, J., Phys. Lett. **3** (1959) 77; Stratonovich, R.D., Dokl. Akad. Nauk., SSSR **115** (1957) 1907 [transl: Soviet Phys. Kokl. **2** (1958) 416]
28. Sugiyama, G. and Koonin, S.E., Ann. Phys. **168** (1986) 1
29. von der Linden, W., Phys. Rep. **220** (1992) 53, and references therein.
30. Hirsch, J.E., Phys. Rev. **B28** (1983) 4059
31. Lawson, R.D., *Theory of the Nuclear Shell Model* (Clarendon Press, Oxford, 1980)
32. Heyde, K., *The Nuclear Shell Model* (Springer, Berlin, 1991)
33. DeShalit, A. and Talmi, I., *Nuclear Shell Theory* (Academic Press, New York, 1963)
34. Brussard, P.J. and Glaudemans, P.M.W., *Shell Model applications in Nuclear Spectroscopy* (North-Holland, Amsterdam, 1977)
35. Kuo, T.T.S. and Brown, G.E., Nucl. Phys. **85** (1966) 40; Kuo, T.T.S., Ann. Rev. Nucl. Sci. **24** (1974) 101
36. Barrett, B.R. and Kirson, M.W., Adv. Nucl. Phys. **6** (1973) 219
37. Jiang, M.W., Machleidt, R., Stout, D.R., and Kuo, T.T.S., Phys. Rev. **C46** (1992) 910
38. Brown, B.A. and Wildenthal, B.H., Ann. Rev. Nucl. Part. Sci. **38** (1988) 29
39. Richter, W.A., Vandermerwe, W.A., Julies, R.E., and Brown, B.A., Nucl. Phys. **A523** (1991) 325
40. Dufour, M. and Zuker, A., preprint (Universite Louis Pasteur, Strasbourg, 1994)

41. Kumar, K. and Baranger, M., Nucl. Phys. **110** (1968) 529; **A122** (1968) 27, 273, 522
42. Etchegoyen, C., Rae, W.D.M., Godwin, N.S., Richter, W.A., Zimmerman, C.H., Brown, B.A., Ormand, W.E., and Winfield, J.S., MSU-NSCL Report **524** (1985)
43. Lanczos, C., Res. Nat. Bur. Stand. **45** (1950) 55
44. Koonin, S.E. and Meredith, D.C., *Computational Physics* (Addison-Wesley, Redwood City, 1990)
45. Caurier, E., Zuker, A.P., Poves, A., and Martinez-Pinedo, G., Phys. Rev. **C50** (1994) 225
46. Caurier, E., Martinez-Pinedo, G., Poves, A., and Zuker, A.P., Phys. Rev. **C52** (1995) R1736
47. Loh, Jr., E.Y. and Gubernatis, J.E., *Electronic Phase Transitions*, ed by W. Hanke, and Yu.V. Kopaev (1992) 177
48. Langanke, K., Dean, D.J., Radha, P.B., Alhassid, Y., and Koonin, S.E., Phys. Rev. **C52** (1995) 718
49. Metropolis, N., Rosenbluth, A., Rosenbluth, M., Teller, A., and Teller, E., J. Chem. Phys. **21** (1953) 1087
50. Dean, D.J., Koonin, S.E., Lang, G.H., Radha, P.B., and Ormand, W.E., Phys. Lett. B317 (1993) 275
51. Condon, E.V. and Shortley, G.H., *The Theory of Atomic Spectra*, Ch. III (Cambridge University Press, 1935).
52. If all single-particle orbits in the model space have the same parity, $\pi = +1$ and the sign rule of Ref. (24) is reproduced. The sign rule of Ref. (24) holds in the Biedenharn-Rose convention, but in the calculation of the two-body matrix elements the spherical harmonics Y_{lm} should be multiplied by i^l.
53. Williams, A.L. *et al.*, Phys. Rev. **C51** (1995) 1144
54. Alford, W.P. *et al.*, Nucl. Phys. **A514** (1990) 49
55. Vetterli, M.C. *et al.*, Phys. Rev. **C40** (1989) 559
56. El-Kateb, S. *et al.*, Phys. Rev. **C49** (1994) 3129
57. Rönnquist, T. *et al.*, Nucl. Phys. **A563** (1993) 225
58. Bertsch, G.F. and Hamomoto, I., Phys. Rev. **C26** (1982) 1323
59. Ericson, M., Figureau, A., and Thevenet, C., Phys. Lett. **45B** (1973) 19; Oser, E. and Rho, M., Phys. Rev. Lett. **42** (1979) 47; Townes, I.S. and Khanna, F.C., Phys. Rev. Lett. **42** (1979) 51; Bohr, A. and Mottelson, B., Phys. Lett. 100B (1981) 10
60. Suraud, E., Gregoire, Ch., and Tamain, B., Prog. Nucl. Part. Phys. **23** (1989) 357
61. Snover, K., Ann. Rev. Nucl. Part. Sci. **36** (1986) 545
62. Alhassid, A., in *New Trends in Nuclear Collective Dynamics*, edited by Y. Abe *et al.* (Springer Verlag, New York, (1991) p. 41-91
63. Egido, J.L. and Ring, P., J. Phys. **G19** (1993) 1; Nucl. Phys. **A388** (1982) 19
64. Dukelsky, J., Poves, A., and Retamosa, J., Phys. Rev. **C44** (1991) 2872
65. Dean, D.J., Radha, P.B., Langanke, K., Alhassid, Y., Koonin, S.E., and Ormand, W.E., Phys. Rev. Lett. **72** (1994) 4066
66. Langanke, K., Dean, D.J., Radha, P.B., and Koonin, S.E., submitted to Nucl. Phys. A
67. Civitarese, O., Dussel, G.G., and Zuker, A.P., Phys. Rev. **C40** (1989) 2900
68. Aufderheide, M.B., Fushiki, I., Woosley, S.E., and Hartmann, D.H., Astrophys. J. Suppl. 91 (1994) 389
69. Fuller, G.A., Fowler, W.A., and Newman, M.J., ApJS **42** (1980) 447; **48** (1982) 279; ApJ **252** (1982) 715; **293** (1985) 1

70. Aufderheide, M.B., Bloom, S.D, Resler, D.A., and Mathews, G.J., Phys. Rev. **C47** (1993) 2961; Phys. Rev. **C48** (1993) 1677
71. Jackson, J.D., *Classical Electrodynamics* (Wiley, New York, 1962).
72. Wilets, L. and Jean, M., Phys. Rev. **102** (1956) 788
73. Vorov, O.K. and Zelevinsky, V.G., Nucl. Phys. A **439** (1985) 207
74. Krips, W. et al., Nucl. Phys. A **529** (1991) 485
75. Otsuka, T., Nucl. Phys. A **557** (1993) 531c
76. Alhassid, Y., Bertsch, G.F., Dean, D.J., and Koonin, S.E., submitted to Phys. Rev. Lett. (1995).
77. Broglia, R., Bes, D.R., and Nilsson, B.R., Phys. Lett. B **50** (1974) 213
78. Wyss, R. and Nazarewicz, W., private communication.
79. Raman, S. *et al.*, Atomic Data and Nuclear Data Tables **36** (1987) 1
80. Radha, P.B., Dean, D.J., Koonin, S.E., Kuo, T.T.S., Langanke, K., Poves, A., Retamosa, J., and Vogel, P., submitted to Phys. Rev. Lett. (September 1995)
81. Vasenko, A.A. *et al.*, Mod. Phys. Lett. **A5** (1990) 1229
82. Avignone, F.T. *et al.*, Phys. Lett. **B256** (1991) 559
83. Beck, M. *et al.*, Phys. Rev. Lett. **70** (1993) 2853; Balysh, A. *et al.* Phys. Lett. **B322** (1994) 176
84. Haxton, W.C. and Stephenson Jr., G.J., Prog. in Part. and Nucl. Phys. **12** (1984) 409
85. Kuo, T.T.S. and Osnes, E., *Lecture Notes in Physics* **364** (Springer-Verlag, Berlin, 1990) 1
86. Caurier, E., Nowacki, F., Poves, A. and Retamosa, J., preprint (Universite Louis Pasteur, Strasbourg; Universidad Autonoma de Madrid (January 1996)
87. Honwa, M., Mizusaki, T., and Otsuka, T., Phys. Rev. Lett. **75** (1995) 1284